Three-dimensional imaging of lipids and metabolites in tissues by nanospray desorption electrospray ionization mass spectrometry

ARTICLE *in* ANALYTICAL AND BIOANALYTICAL CHEMISTRY · NOVEMBER 2014

Impact Factor: 3.44 · DOI: 10.1007/s00216-014-8174-0 · Source: PubMed

8 AUTHORS, INCLUDING:

Ingela Lanekoff
Uppsala University
21 PUBLICATIONS **257** CITATIONS
SEE PROFILE

Kristin E Burnum-Johnson
Pacific Northwest National Laboratory
33 PUBLICATIONS **698** CITATIONS
SEE PROFILE

Jeeyeon Cha
Vanderbilt University
22 PUBLICATIONS **350** CITATIONS
SEE PROFILE

Sudhansu K Dey
Cincinnati Children's Hospital Medical Center
470 PUBLICATIONS **23,710** CITATIONS
SEE PROFILE

Anal Bioanal Chem
DOI 10.1007/s00216-014-8174-0

RESEARCH PAPER

Three-dimensional imaging of lipids and metabolites in tissues by nanospray desorption electrospray ionization mass spectrometry

Ingela Lanekoff · Kristin Burnum-Johnson · Mathew Thomas · Jeeyeon Cha · Sudhansu K. Dey · Pengxiang Yang · Maria C. Prieto Conaway · Julia Laskin

Received: 5 August 2014 / Revised: 3 September 2014 / Accepted: 8 September 2014

Abstract Three-dimensional (3D) imaging of tissue sections is a new frontier in mass spectrometry imaging (MSI). Here, we report on fast 3D imaging of lipids and metabolites associated with mouse uterine decidual cells and embryo at the implantation site on day 6 of pregnancy. 2D imaging of 16–20 serial tissue sections deposited on the same glass slide was performed using nanospray desorption electrospray ionization (nano-DESI)—an ambient ionization technique that enables sensitive localized analysis of analytes on surfaces without special sample pretreatment. In this proof-of-principle study, nano-DESI was coupled to a high-resolution Q-Exactive instrument operated at high repetition rate of >5 Hz with moderate mass resolution of 35,000 ($m/\Delta m$ at m/z 200), which enabled acquisition of the entire 3D image with a spatial resolution of ~150 μm in less than 4.5 h. The results demonstrate localization of acetylcholine in the primary decidual zone (PDZ) of the implantation site throughout the depth of the tissue examined, indicating an important role of this signaling molecule in decidualization. Choline and phosphocholine—metabolites associated with cell growth—are enhanced in the PDZ and abundant in other cellular regions of the implantation site. Very different 3D distributions were obtained for fatty acids (FA), oleic acid and linoleic acid (FA 18:1 and FA 18:2), differing only by one double bond. Localization of FA 18:2 in the PDZ indicates its important role in decidualization while FA 18:1 is distributed more evenly throughout the tissue. In contrast, several lysophosphatidylcholines (LPC) observed in this study show donut-like distributions with localization around the PDZ. Complementary distributions with minimal overlap were observed for LPC 18:0 and FA 18:2 while the 3D image of the potential precursor phosphatidylcholine 36:2 (PC 36:2) showed a significant overlap with both LPC 18:0 and FA 18:2.

Keywords Three-dimensional (3D) imaging mass spectrometry · Nanospray desorption electrospray ionization (nano-DESI) · Mouse embryo · Phospholipids · Metabolites

Published in the topical collection *Mass Spectrometry Imaging* with guest editors Andreas Römpp and Uwe Karst.

Electronic supplementary material The online version of this article (doi:10.1007/s00216-014-8174-0) contains supplementary material, which is available to authorized users.

I. Lanekoff · J. Laskin (✉)
Physical Sciences Division, Pacific Northwest National Laboratory, Richland, WA 99354, USA
e-mail: Julia.Laskin@pnnl.gov

K. Burnum-Johnson
Biological Sciences Division, Pacific Northwest National Laboratory, Richland, WA 99354, USA

M. Thomas
Computational Sciences and Mathematics Division, Pacific Northwest National Laboratory, Richland, WA 99354, USA

J. Cha · S. K. Dey
Division of Reproductive Sciences, The Perinatal Institute, Cincinnati Children's Hospital Medical Center, University of Cincinnati College of Medicine, Cincinnati, OH 45229, USA

P. Yang · M. C. Prieto Conaway
Thermo Fisher Scientific, San Jose, CA 95134, USA

Introduction

Mass spectrometry imaging (MSI) enables molecular imaging of ionizable molecules in biological samples with a spatial

Published online: 14 November 2014

resolution approaching that of histological imaging [1–4]. This capability has been extensively used for spatially resolved analysis of biological systems [5–15]. For example, MSI has been widely used for obtaining molecular signatures of diseases [16–21], studying metabolic processes in plant tissues [22–26], understanding metabolic exchange between microbial communities [27–29], and localizing drugs in tissues [30–34, 9, 12, 35]. Three-dimensional (3D) molecular imaging has been identified as an emerging frontier in MSI [36]. High spatial and depth resolution have been achieved in 3D imaging of biological samples using secondary ion mass spectrometry (SIMS) [37–40]. 3D SIMS imaging experiments use alternating cycles of 2D imaging in the static regime and in situ ion sputtering of the top layer of material from the surface [37, 41–43, 38, 44, 39]. This approach has been used for 3D imaging of single cells with a lateral resolution down to 300 nm and a depth resolution of 100 nm [43] and for depth profiling of rat brain tissue sections using a C_{60}^+ sputter source [44]. Despite the success of 3D SIMS imaging of biological samples, data interpretation is often complicated by the facile fragmentation of molecules in SIMS analysis.

Soft ionization techniques enable 2D and 3D imaging of intact biomolecules in biological samples [5, 6, 45, 8, 46, 47, 9–14, 48]. 3D imaging has been accomplished using matrix-assisted laser desorption ionization (MALDI) [49–54, 15], desorption electrospray ionization (DESI) [55, 56], and laser ablation electrospray ionization (LAESI) [57]. In these experiments, 2D imaging of multiple mouse tissue sections using traditional approaches was followed by data registration and 3D reconstruction of the resulting images. Because the analysis time increases with an increase in spatial resolution, 3D imaging experiments based on soft ionization techniques are typically performed with a spatial and vertical resolution of >100 μm. Rapid image acquisition and minimal sample pretreatment prior to analysis are necessary for increasing the throughput of the 3D MSI experiments [58]. When coupled to a fast mass analyzer, ambient surface ionization techniques, that do not require matrix application or any other special sample pretreatment, are ideally suited for high-throughput 3D imaging experiments.

Herein, we report on 3D imaging of decidualizing mouse uterine tissue sections using nanospray desorption electrospray ionization (nano-DESI) MSI [59]—a recently developed ambient ionization technique that relies on localized liquid extraction of analyte molecules from complex samples followed by efficient transfer of the extracted material to a mass spectrometer inlet and soft ionization by nanoelectrospray prior to MS analysis. Nano-DESI has been previously used for chemical analysis and imaging of complex biological and environmental samples, evaluation of matrix effects, and quantification of lipids and metabolites in biological tissue sections [60–64, 28, 65, 66, 29, 67–72]. When coupled with high-resolution mass spectrometry, nano-DESI enables sensitive analysis and imaging of hundreds of ionizable molecules in complex samples without special sample pretreatment. Furthermore, the solvent composition may be optimized for the more efficient extraction and ionization of different classes of compounds [62]. In this study, nano-DESI MSI was performed using a high-resolution mass spectrometer operated at a high repetition rate, which enabled rapid acquisition of 3D images of biological tissues.

Experimental section

Tissue collection and handling

All mice used in this investigation were housed in the Cincinnati Children's Hospital Medical Center Animal Care Facility according to National Institutes of Health and institutional guidelines for the use of laboratory animals. All protocols of the present study were reviewed and approved by Cincinnati Children's Hospital Research Foundation Institutional Animal Care and Use Committee. Adult CD-1 mice were purchased from Charles River Laboratory (Raleigh, NC). Females were mated with fertile males of the same strain to induce pregnancy (day 1 of pregnancy = vaginal plug). Embryo implantation sites on day 6 of pregnancy were dissected from uteri and snap frozen. Successive 12-μm-thick sections of ~4–5 mm in diameter from the central part of the tissue were mounted onto ~20×16 mm areas on glass slides precoated with poly-L-lysine; each slide contained 16 to 20 sections per implantation site. For this first study, the whole tissue was not utilized due to its small size. Figure 1a shows an optical image of one of the slides examined in this

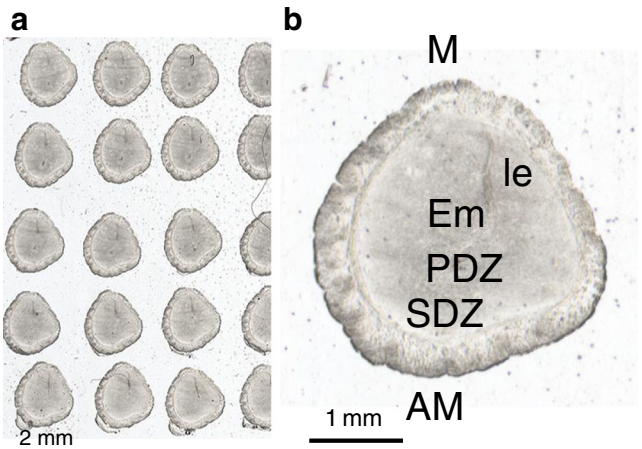

Fig. 1 **a** Optical image of one of the glass slides containing sequential 12-μm-thick mouse uterine tissue sections examined in this study; **b** enlarged optical image of one of the sections showing the mesometrial pole (*M*), antimesometrial pole (*AM*), embryo (*Em*), primary decidual zone (*PDZ*), secondary decidual zone (*SDZ*), and luminal epithelium (*le*). *Lateral scale bar* is 2 mm for panel **a** and 1 mm for panel **b**. The same orientation is used in all ion images and supplementary movies presented herein

study. Slides were stored at −80 °C. The slides were equilibrated to room temperature prior to analysis.

Nano-DESI imaging

A custom-designed nano-DESI imaging source was mounted onto a Q-Exactive Orbitrap mass spectrometer (Thermo Scientific, Bremen, Germany). The nano-DESI probe was assembled using a specially designed capillary holder, in which two fused silica capillaries (ID 50 μm, OD 150 μm, Polymicro Technologies, LLC, Phoenix, AZ) were placed in precisely machined grooves and sandwiched between two plastic plates. The capillaries were positioned in the holder under a microscope and fixed by tightening set screws connecting the two plates [67]. A custom-made nano-DESI sample holder attached to a motorized XYZ stage (Newport Corp., Irvine, CA) was controlled by custom-designed LabVIEW software as described in our previous study [65]. A 9:1 methanol:water mixture was used as a nano-DESI solvent. The solvent was delivered via a syringe pump (Legato 180, KD Scientific) through the primary capillary to the sample at a flow rate of 0.5 μl/min. Ions were produced by nanoelectrospray from the secondary capillary at the mass spectrometer inlet by applying a high voltage of 3.0 kV to a stainless steel union housing the primary capillary. The heated capillary was kept at 250 °C.

3D images were acquired for implantation sites obtained from three different animals by moving the sample under the nano-DESI probe in the *x*-direction in lines at 200 μm/s and stepping between the individual lines by 154 μm in the *y*-direction. In a typical experiment, about 100 lines were acquired over a ~20×16 mm area on the glass slide containing on average 20 successive tissue sections thereby creating ion images for all the sections in one experiment. The total acquisition time for one 3D image was around 4.5 h. The Q-Exactive instrument was operated in a positive mode with a mass resolution of 35,000 ($m/\Delta m$ at m/z 200) and an average acquisition rate of 5.2 Hz. Higher mass resolution was not necessary for these proof-of-principle experiments.

Tandem mass spectrometry (MS/MS) experiments were performed on molecules observed in nano-DESI spectra using data dependent acquisition, in which a full-scan MS is followed by MS/MS of the most abundant ions. The mass range for the full-scan MS was m/z 83.4 to 1251 with 35,000 resolving power ($m/\Delta m$ at m/z 200). MS/MS spectra were acquired with a resolving power of 17,500. This experiment enables selective acquisition of data without user intervention, which is important in applications such as automated structural identification, sequence determination and unknown compound confirmation. The Q-Exactive Orbitrap mass spectrometer operates at a mass accuracy of <3 ppm with external calibration. Dynamic exclusion of 50 s was used in this study. Dynamic exclusion puts a mass into a temporary exclusion list after its MS/MS spectrum is acquired, providing the opportunity to collect MS/MS information on less abundant components that may otherwise not be examined. Data was acquired in positive ion and in profile mode. Other acquisition parameters were maximum injection time of 50 ms for full-scan MS and 100 ms for MS/MS. Each MS/MS spectrum was acquired with a mass isolation window of 2 amu using higher collision energy dissociation (HCD), during which the nominal collision energy was ramped in the range of 24–36 V.

Data analysis

Imaging datasets were visualized and processed using the customized imaging software, MSI QuickView [73]. MSI QuickView enables real-time visualization and the post-processing of imaging datasets acquired as a collection of line scans across the sample. Specifically, it enables generation of ion images for multiple selected m/z values and m/z ranges, visualization of spectra and extracted ion chronograms (time-dependent signal of a selected m/z), image classification, normalization, and correction for variations in the acquisition time of individual spectra [65]. Since individual tissue sections where imaged side-by-side in this study, a semi-automated approach was developed to separate and register the 2D sections to generate the final 3D images. The optical image was first warped to bring it into the coordinate system of the 2D ion image. This was performed by selecting identical pair of points in both images and then using the spatial transformation function in MATLAB. Individual tissue sections were then cropped out from the warped optical image. Finally, the initial section was used as the reference and the adjacent sections were warped into its coordinate system by selecting identical points on both images using the 2D spatial transformation function in MATLAB. The registration parameters were saved and used to automatically register all 2D ion images, which were loaded into the open-source visualization and analysis toolkit, ImageJ (http://imagej.nih.gov/ij/), for 3D visualization. All ion images shown in this study were normalized to the total ion current (TIC).

Results and discussion

Figure 1a shows an optical image of one of the glass slides used in the 3D imaging experiments; Fig 1b shows a close up of a representative mouse uterine section examined in this study. The same orientation is used in all ion images and supplementary movies presented herein. The attachment of the blastocyst to the uterine luminal epithelium (le) at the antimesometrial (AM) pole initiates decidualization of underlying stromal cells at this site [74]. In contrast, the mesometrial (M) pole is the future site of placentation. Previous studies

showed that differences in the biological processes occurring at the AM and M poles result in distinct localization of proteins and lipids at the implantation site. In this study, we examined spatial distribution of ionizable and relatively abundant lipids and metabolites associated with the development of the embryo-decidua unit on day 6 of pregnancy using 3D nano-DESI imaging. 3D images were acquired for implantation sites from three different animals. Similar results were obtained in all three data sets.

Figure 2 shows a representative mass spectrum obtained by averaging a line scan across one of the tissue sections; a typical single-pixel spectrum is shown in Fig S1 of the Electronic Supplementary Material (ESM). The spectrum contains abundant metabolites and lipids. Peak assignment was performed based on the accurate mass measurement and by comparing MS/MS spectra of the isolated precursor ions (selected MS/MS spectra are shown in Figs S2–S12 of the ESM) with METLIN database (http://metlin.scripps.edu/) and with published MS/MS data. The lower *m/z* region of the spectrum is dominated by signals of choline at *m/z* 104.107, acetylcholine at *m/z* 146.117, $[M+K]^+$ ion of creatine at *m/z* 170.032, $[M+K]^+$ ion of carnitine at *m/z* 200.068, and $[M+K]^+$ ion of glycerophosphocholine at *m/z* 296.065. Abundant glycerophospholipids, dominated by phosphatidylcholine (PC) species, are observed at higher *m/z*; peaks corresponding to a sodium adduct of lysophosphatidylcholine (LPC) 16:0 at *m/z* 534.295, $[M+K]^+$ ion of PC 34:1 at *m/z* 798.5394, $[M+K]^+$ ion of PC 36:2 at *m/z* 824.5551, and $[M+K]^+$ ion of PC 38:4 at *m/z* 848.5551 are labeled in the spectrum.

Figure 3 shows 2D ion images of acetylcholine at *m/z* 146.118, choline at *m/z* 104.107, and $[M+K]^+$ of phosphocholine at *m/z* 222.028, and snapshots of the corresponding 3D images. The actual 3D images are shown in Movies S1–S3 of the ESM. In agreement with our recent tandem mass spectrometric (MS/MS) imaging study, acetylcholine is localized to the avascular primary decidual zone (PDZ) [67]. In contrast, while choline and phosphocholine show enhanced signal in the PDZ, they are also observed in other cellular regions of the implantation sites. Choline, a precursor of acetylcholine, is an essential nutrient necessary for biosynthesis of phospholipids. In the PDZ, an increase in choline and phosphocholine could contribute to cellular differentiation and intracellular signal transduction. Acetylcholine is an important signaling molecule known to be involved in gastrulation (an early stage of embryo development that precedes the formation of individual organs or organogenesis) [75]. For example, Laasberg and Neuman observed a sharp increase in the activity of acetylcholinesterase (AChE) (an enzyme responsible for conversion of acetylcholine into choline) in gastrulating chicken embryos [76]. Furthermore, Gustafson and Toneby suggested that acetylcholine initiates morphogenetic cell movements in sea urchin embryos [77], while Drews et al. correlated the enhanced activity of AChE with morphogenesis [78]. However, AChE was not detected using immunoblot in a study focused on choline uptake and metabolism in mouse embryos [79]. The observed specific localization of acetylcholine to the PDZ indicates that this molecule plays an important role unique to decidual cell signaling.

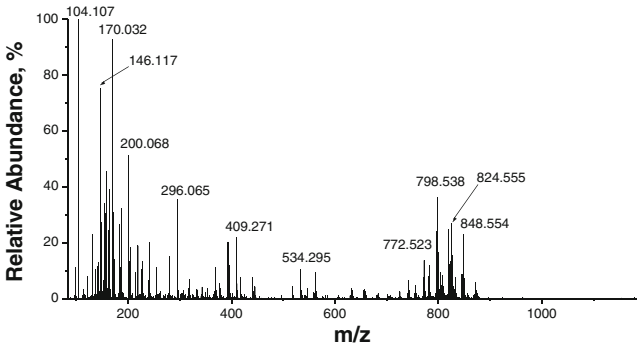

Fig. 2 An average mass spectrum showing peaks corresponding to metabolites and lipids observed in a typical mouse uterine tissue section (see text for detailed description of the labeled peaks)

Fatty acid (FA) and phospholipid synthesis are critically important in embryonic development. Chirala et al. demonstrated that homozygous mutant mouse blastocysts lacking fatty acid synthase die before implantation, while heterozygous embryos die at different stages of development [80]. Although MSI has been extensively used for imaging of endogenous lipids in tissue sections, little work has been done on the spatial localization of FAs. In MALDI MSI, the lower *m/z* region is dominated by matrix peaks making it difficult to detect FAs due to overlapping peaks. Furthermore, in positive ion mode, FA signals in MSI experiments are typically less abundant than phospholipid signals. Ambient nano-DESI imaging used in this study is suitable for simultaneous visualization of lipids and metabolites with high sensitivity and low chemical background [64–66]. Figure 4 shows snapshots of 3D images where the potassium adducts of FA 18:2 at *m/z* 319.204 and lysophosphatidylcholine (LPC) 18:0 at *m/z* 562.327 are overlaid. The corresponding 2D images and snapshots of 3D images of $[FA\ 18:2+K]^+$, $[LPC\ 18:0+K]^+$, and potassium adduct of PC 36:2 at *m/z* 824.555 are shown in Fig S13 and in Movies S4–S6 of the ESM. FA 18:2, LPC 18:0, and PC 36:2 are part of the same metabolic pathway, in which PC 36:2 is synthesized from FA 18:2 and LPC 18:0. The intensity of PC 36:2 is enhanced at the AM pole, consistent with the earlier MALDI MSI study by Burnum et al. which showed the ion images of PC (18:0/18:2) [81]. In contrast, the intensity of LPC 18:0 is significantly decreased in the PDZ region of the AM pole resulting in a donut-like shape of the 3D image. Only a small overlap of the LPC 18:0 and FA 18:2 signals is observed in the 3D images. The overlapping region is shown in Fig 4 in purple, while the signal of PC 36:2, enhanced at the AM pole, is observed throughout the tissue. By

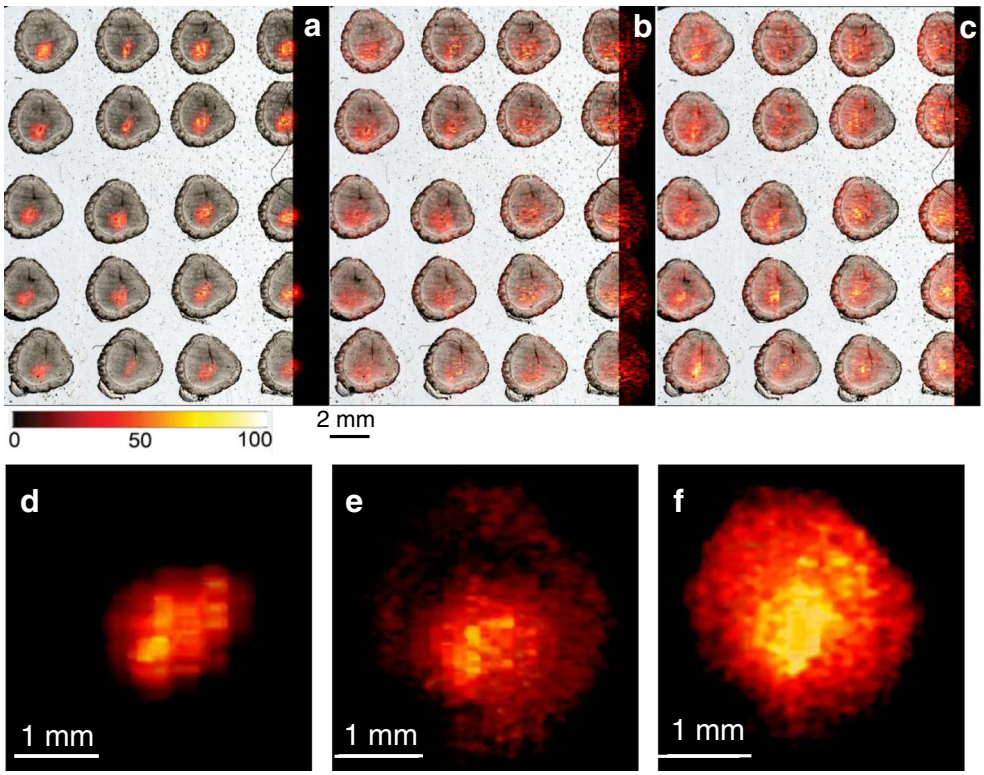

Fig. 3 Selected 2D ion images (**a**–**c**) and snapshots of 3D images (**d**–**f**) of **a**, **d** acetylcholine at *m*/*z* 146.118, **b**, **e** choline at *m*/*z* 104.107, **c**, **f** phosphocholine at *m*/*z* 222.028. *Lateral scale bar* is 2 mm for panels **a**–**c** and 1 mm for panels **d**–**f**. *Intensity scale bar* ranging from 0 (*black*) to 100 % (*light yellow*) signal intensity of an individual peak

visualizing ion intensities, MSI provides information on the biological processes occurring in living systems. However, the interpretation of ion images must be done with caution as they may be affected by "matrix effects" (signal suppression in direct ionization of complex analyte mixtures). Matrix effects in nano-DESI MSI have been discussed in detail in our recent study [71], in which we also introduced an approach that efficiently compensates for matrix effects by adding

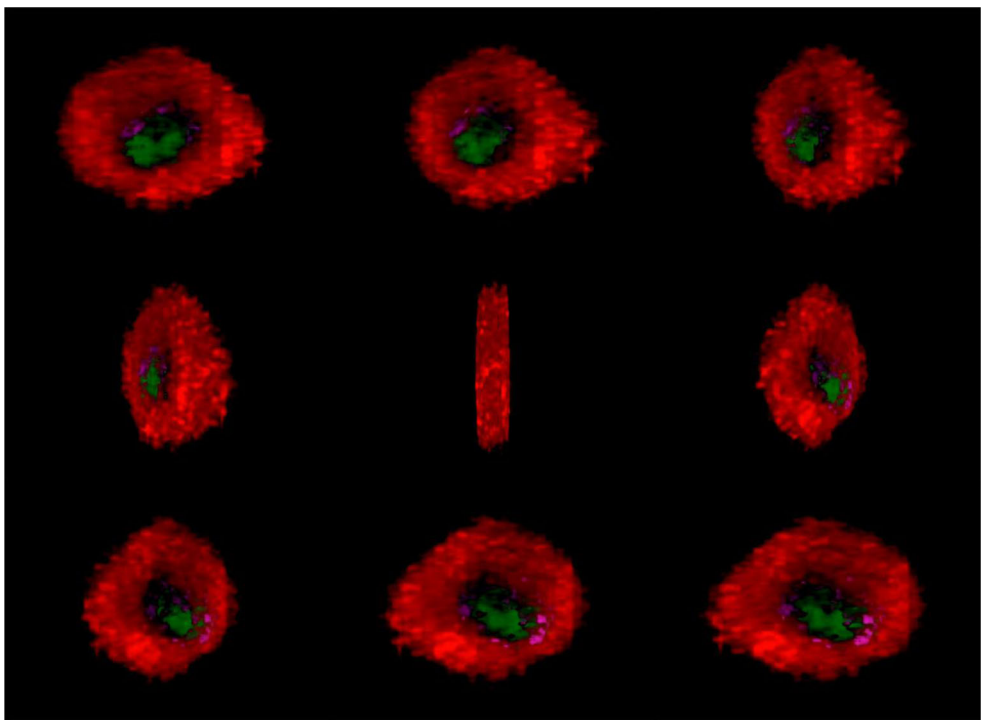

Fig. 4 Snapshots of overlaid 3D images of $[FA\ 18:2+K]^+$ at *m*/*z* 319.204 (*green*) and $[LPC\ 18:0+K]^+$ at *m*/*z* 562.327 (*red*); the area in which both signals are present is shown in *purple*. The corresponding 2D data are shown in Fig S13 of the supplementary material

appropriate standards to the nano-DESI solvent and normalizing ion intensities of endogenous signals to the intensity of the standard. Of note, similar 3D images were obtained in this study when ion intensities were normalized to TIC and to the internal standard indicating that the observed 3D images of ionizable compounds closely represent the actual concentration gradients in the system. The 3D images of FA 18:2 and LPC 18:0 indicate changes in metabolic fluxes resulting in formation of these species in different cellular regions of the uterus.

FA 18:1 and FA 18:2 have very similar ionization properties and it is reasonable to compare ion distributions of these species as they are expected to be suppressed or enhanced to the same extent by matrix effect. The signal of FA 18:2 is significantly enhanced in the PDZ region of the AM pole and almost completely undetectable in other parts of the mouse uterine tissue. In contrast, the signal of FA 18:1 at *m/z* 321.218 (Movie S7) is almost uniformly distributed along the uterus indicating that the degree of unsaturation has a significant effect on the distribution of FAs at this stage of embryo development. This assertion is further supported by the differences in the spatial localization of LPC 18:0 (Fig 4) and LPC 18:1 at *m/z* 560.310 (Movie S8), which also have similar ionization properties. The signal corresponding to LPC 18:1 is enhanced in the M pole and the spatial distribution is almost complementary to the spatial distribution of LPC 18:0. It is interesting to compare our observations with the immunostaining data reported by Chirala et al. [80]. Specifically, they demonstrated that on day 6 of pregnancy, fatty acid synthase (FAS) responsible for FA synthesis is expressed in the decidual cells surrounding the embryo and the embryonic and extraembryonic endoderm. Furthermore, Tian et al. showed that, on day 7 of pregnancy in mice, fatty acid binding protein 4 (FABP4) involved in the transfer of FAs between extra- and intracellular membranes is expressed in the decidua [82]. The enhanced abundance of FA 18:2 in the PDZ is consistent with the enhanced expression of proteins involved in the synthesis and transport of FAs at this early stage of embryo development.

Conclusions

In this study, we present the first 3D imaging of mouse uterine sections on day 6 of pregnancy using nano-DESI imaging mass spectrometry. By imaging ~20 mouse uterine tissue sections mounted on the same glass slide using the high repetition rate of the Q-Exactive, 3D images with a spatial resolution of 150 μm in Y and a vertical resolution of 12 μm were acquired in less than 4.5 h. This relatively short acquisition time enables high-throughput 3D imaging and reduces possible experimental artifacts related to lipid and metabolite degradation during the MSI experiment.

MSI provides insights into lipid and metabolite distributions in biological systems which are determined by many complex processes. The ability to map distributions of ionizable lipids and metabolites in 3D, in a fairly high-throughput manner and with high sensitivity, enables comparison of spatially resolved molecular signatures with other spatially resolved measurements such as immunostaining, in situ hybridization, magnetic resonance spectroscopy, or radiolabeling. The 3D images in this study demonstrated differences in ion distributions of choline, phosphocholine, and acetylcholine. Tight localization of abundant acetylcholine ions in the PDZ indicates that this molecule is involved in decidual cell signaling. In contrast, the spatial distribution of choline and phosphocholine mimics the spatial distribution of ionizable phospholipids, which is consistent with the role of these small molecules as precursors in the synthesis of PC. In addition, we found that small differences in the composition of the fatty acid tail have a significant effect on the spatial distribution of FAs and lipids and that the enhanced abundance of FA 18:2 in the PDZ suggests its special role in the decidualization process on day 6 of pregnancy.

Acknowledgments The research described in this paper is part of the Chemical Imaging Initiative, at Pacific Northwest National Laboratory (PNNL). It was conducted under the Laboratory Directed Research and Development Program at PNNL a multiprogram national laboratory operated by Battelle for the US Department of Energy (DOE) under Contract DE-AC05-76RL01830. The research was performed at EMSL, a national scientific user facility sponsored by the DOE's Office of Biological and Environmental Research and located at PNNL. This work was partially supported by NIH grants (HD068524 and DA06668) and the March of Dimes to SKD. JC is supported by a Ruth L. Kirschstein Predoctoral NRSA Fellowship (F30AG040858).

A single-pixel MS spectrum, MS/MS spectra of selected compounds discussed in the paper, selected 2D images, and the 3D image reconstruction can be found in the Electronic Supplementary Material.

References

1. Luxembourg SL, Mize TH, McDonnell LA, Heeren RMA (2004) High-spatial resolution mass spectrometric imaging of peptide and protein distributions on a surface. Anal Chem 76(18):5339–5344. doi:10.1021/ac049692q
2. Setou M, Kurabe N (2011) Mass microscopy: high-resolution imaging mass spectrometry. J Electron Microsc 60(1):47–56. doi:10.1093/jmicro/dfq079
3. Yang JH, Caprioli RM (2011) Matrix sublimation/recrystallization for imaging proteins by mass spectrometry at high spatial resolution. Anal Chem 83(14):5728–5734. doi:10.1021/ac200998a
4. Rompp A, Spengler B (2013) Mass spectrometry imaging with high resolution in mass and space. Histochem Cell Biol 139(6):759–783. doi:10.1007/s00418-013-1097-6
5. Cornett DS, Reyzer ML, Chaurand P, Caprioli RM (2007) MALDI imaging mass spectrometry: molecular snapshots of biochemical systems. Nat Methods 4(10):828–833. doi:10.1038/nmeth1094

6. McDonnell LA, Heeren RMA (2007) Imaging mass spectrometry. Mass Spectrom Rev 26(4):606–643. doi:10.1002/mas.20124
7. Burnum KE, Frappier SL, Caprioli RM (2008) Matrix-assisted laser desorption/ionization imaging mass spectrometry for the investigation of proteins and peptides. Annu Rev Anal Chem 1:689–705. doi:10.1146/annurev.anchem.1.031207.112841
8. Walch A, Rauser S, Deininger SO, Hofler H (2008) MALDI imaging mass spectrometry for direct tissue analysis: a new frontier for molecular histology. Histochem Cell Biol 130(3):421–434. doi:10.1007/s00418-008-0469-9
9. Greer T, Sturm R, Li LJ (2011) Mass spectrometry imaging for drugs and metabolites. J Proteome 74(12):2617–2631. doi:10.1016/j.jprot.2011.03.032
10. Watrous JD, Alexandrov T, Dorrestein PC (2011) The evolving field of imaging mass spectrometry and its impact on future biological research. J Mass Spectrom 46(2):209–222. doi:10.1002/jms.1876
11. Chaurand P (2012) Imaging mass spectrometry of thin tissue sections: a decade of collective efforts. J Proteome 75(16):4883–4892. doi:10.1016/j.jprot.2012.04.005
12. Prideaux B, Stoeckli M (2012) Mass spectrometry imaging for drug distribution studies. J Proteome 75(16):4999–5013. doi:10.1016/j.jprot.2012.07.028
13. Gode D, Volmer DA (2013) Lipid imaging by mass spectrometry—a review. Analyst 138(5):1289–1315. doi:10.1039/C2AN36337B
14. Wu CP, Dill AL, Eberlin LS, Cooks RG, Ifa DR (2013) Mass spectrometry imaging under ambient conditions. Mass Spectrom Rev 32(3):218–243. doi:10.1002/mas.21360
15. Crecelius AC, Cornett DS, Caprioli RM, Williams B, Dawant BM, Bodenheimer B (2005) Three-dimensional visualization of protein expression in mouse brain structures using imaging mass spectrometry. J Am Soc Mass Spectrom 16(7):1093–1099. doi:10.1016/j.jasms.2005.02.026
16. Chaurand P, Schwartz SA, Caprioli RM (2004) Assessing protein patterns in disease using imaging mass spectrometry. J Proteome Res 3(2):245–252. doi:10.1021/pr0341282
17. Touboul D, Roy S, Germain DP, Chaminade P, Brunelle A, Laprevote O (2007) MALDI-TOF and cluster-TOF-SIMS imaging of Fabry disease biomarkers. Int J Mass Spectrom 260(2–3):158–165. doi:10.1016/j.ijms.2006.09.027
18. Seeley EH, Caprioli RM (2008) Imaging mass spectrometry: towards clinical diagnostics. Proteomics Clin Appl 2(10–11):1435–1443. doi:10.1002/prca.200800013
19. Eberlin LS, Liu XH, Ferreira CR, Santagata S, Agar NYR, Cooks RG (2011) Desorption electrospray ionization then MALDI mass spectrometry imaging of lipid and protein distributions in single tissue sections. Anal Chem 83(22):8366–8371. doi:10.1021/ac202016x
20. Girod M, Shi YZ, Cheng JX, Cooks RG (2011) Mapping lipid alterations in traumatically injured rat spinal cord by desorption electrospray ionization imaging mass spectrometry. Anal Chem 83(1):207–215. doi:10.1021/ac102264z
21. Zaima N, Sasaki T, Tanaka H, Cheng XW, Onoue K, Hayasaka T, Goto-Inoue N, Enomoto H, Unno N, Kuzuya M, Setou M (2011) Imaging mass spectrometry-based histopathologic examination of atherosclerotic lesions. Atherosclerosis 217(2):427–432. doi:10.1016/j.atherosclerosis.2011.03.044
22. Lee YJ, Perdian DC, Song ZH, Yeung ES, Nikolau BJ (2012) Use of mass spectrometry for imaging metabolites in plants. Plant J 70(1):81–95. doi:10.1111/j.1365-313×.2012.04899.×
23. Li Y, Shrestha B, Vertes A (2007) Atmospheric pressure molecular imaging by infrared MALDI mass spectrometry. Anal Chem 79(2):523–532. doi:10.1021/ac061577n
24. Kaspar S, Peukert M, Svatos A, Matros A, Mock HP (2011) MALDI-imaging mass spectrometry—an emerging technique in plant biology. Proteomics 11(9):1840–1850. doi:10.1002/pmic.201000756
25. Lunsford KA, Peter GF, Yost RA (2011) Direct matrix-assisted laser desorption/ionization mass spectrometric imaging of cellulose and hemicellulose in populus tissue. Anal Chem 83(17):6722–6730. doi:10.1021/ac2013527
26. Muller T, Oradu S, Ifa DR, Cooks RG, Krautler B (2011) Direct plant tissue analysis and imprint imaging by desorption electrospray ionization mass spectrometry. Anal Chem 83(14):5754–5761. doi:10.1021/ac201123t
27. Watrous JD, Dorrestein PC (2011) Imaging mass spectrometry in microbiology. Nat Rev Micro 9(9):683–694
28. Watrous J, Roach P, Alexandrov T, Heath BS, Yang JY, Kersten RD, van der Voort M, Pogliano K, Gross H, Raaijmakers JM, Moore BS, Laskin J, Bandeira N, Dorrestein PC (2012) Mass spectral molecular networking of living microbial colonies. Proc Natl Acad Sci U S A 109(26):E1743–E1752. doi:10.1073/pnas.1203689109
29. Lanekoff I, Geydebrekht O, Pinchuk GE, Konopka AE, Laskin J (2013) Spatially resolved analysis of glycolipids and metabolites in living Synechococcus sp PCC 7002 using nanospray desorption electrospray ionization. Analyst 138(7):1971–1978. doi:10.1039/c3an36716a
30. Reyzer ML, Hsieh Y, Ng K, Korfmacher WA, Caprioli RM (2003) Direct analysis of drug candidates in tissue by matrix-assisted laser desorption/ionization mass spectrometry. J Mass Spectrom 38(10):1081–1092. doi:10.1002/jms.525
31. Stoeckli M, Staab D, Schweitzer A (2007) Compound and metabolite distribution measured by MALDI mass spectrometric imaging in whole-body tissue sections. Int J Mass Spectrom 260(2–3):195–202. doi:10.1016/j.ijms.2006.10.007
32. Kertesz V, Van Berkel GJ, Vavrek M, Koeplinger KA, Schneider BB, Covey TR (2008) Comparison of drug distribution images from whole-body thin tissue sections obtained using desorption electrospray ionization tandem mass spectrometry and autoradiography. Anal Chem 80(13):5168–5177. doi:10.1021/ac800546a
33. Wiseman JM, Ifa DR, Zhu YX, Kissinger CB, Manicke NE, Kissinger PT, Cooks RG (2008) Desorption electrospray ionization mass spectrometry: imaging drugs and metabolites in tissues. Proc Natl Acad Sci U S A 105(47):18120–18125. doi:10.1073/pnas.0801066105
34. Nilsson A Fehniger TE. Gustavsson L. Andersson M. Kenne K. Marko-Varga G. Andren PE (2010) Fine mapping the spatial distribution and concentration of unlabeled drugs within tissue microcompartments using imaging mass spectrometry. PLoS One 5 (7). doi:10.1371/journal.pone.0011411
35. Shahidi-Latham SK, Dutta SM, Prieto Conaway MC, Rudewicz PJ (2012) Evaluation of an accurate mass approach for the simultaneous detection of drug and metabolite distributions via whole-body mass spectrometric imaging. Anal Chem 84(16):7158–7165. doi:10.1021/ac3015142
36. Seeley EH, Caprioli RM (2012) 3D imaging by mass spectrometry: a new frontier. Anal Chem 84(5):2105–2110. doi:10.1021/ac2032707
37. Cheng J, Wucher A, Winograd N (2006) Molecular depth profiling with cluster ion beams. J Phys Chem B 110(16):8329–8336. doi:10.1021/jp0573341
38. Delcorte A (2008) On the road to high-resolution 3D molecular imaging. Appl Surf Sci 255(4):954–958. doi:10.1016/j.apsusc.2008.05.111
39. Fletcher JS, Vickerman JC (2010) A new SIMS paradigm for 2D and 3D molecular imaging of bio-systems. Anal Bioanal Chem 396(1):85–104. doi:10.1007/s00216-009-2986-3
40. Vickerman JC (2011) Molecular imaging and depth profiling by mass spectrometry-SIMS, MALDI or DESI? Analyst 136(11):2199–2217. doi:10.1039/c1an00008j
41. Gillen G, Fahey A, Wagner M, Mahoney C (2006) 3D molecular imaging SIMS. Appl Surf Sci 252(19):6537–6541. doi:10.1016/j.apsusc.2006.02.235

42. Breitenstein D, Rommel CE, Möllers R, Wegener J, Hagenhoff B (2007) The chemical composition of animal cells and their intracellular compartments reconstructed from 3D mass spectrometry. Angew Chem Int Ed 46(28):5332–5335. doi:10.1002/anie.200604468
43. Fletcher JS, Lockyer NP, Vaidyanathan S, Vickerman JC (2007) TOF-SIMS 3D biomolecular imaging of Xenopus laevis oocytes using buckminsterfullerene (C-60) primary ions. Anal Chem 79(6):2199–2206. doi:10.1021/ac061370u
44. Jones EA, Lockyer NP, Vickerman JC (2008) Depth profiling brain tissue sections with a 40 keV C-60(+) primary ion beam. Anal Chem 80(6):2125–2132. doi:10.1021/ac702127q
45. Reyzer ML, Caprioli RM (2007) MALDI-MS-based imaging of small molecules and proteins in tissues. Curr Opin Chem Biol 11(1):29–35. doi:10.1016/j.cbpa.2006.11.035
46. Esquenazi E, Yang Y-L, Watrous J, Gerwick WH, Dorrestein PC (2009) Imaging mass spectrometry of natural products. Nat Prod Rep 26(12):1521–1534. doi:10.1039/B915674G
47. Andersson M, Andren P, Caprioli RM (2010) MALDI imaging and profiling mass spectrometry in neuroproteomics. In: Alzate O (ed) Neuroproteomics. CRC, Boca Raton (FL)
48. Ifa DR, Wu CP, Ouyang Z, Cooks RG (2010) Desorption electrospray ionization and other ambient ionization methods: current progress and preview. Analyst 135(4):669–681. doi:10.1039/b925257f
49. Andersson M, Groseclose MR, Deutch AY, Caprioli RM (2008) Imaging mass spectrometry of proteins and peptides: 3D volume reconstruction. Nat Methods 5(1):101–108. doi:10.1038/nmeth1145
50. Chen RB, Hui LM, Sturm RM, Li LJ (2009) Three dimensional mapping of neuropeptides and lipids in crustacean brain by mass spectral imaging. J Am Soc Mass Spectrom 20(6):1068–1077. doi:10.1016/j.jasms.2009.01.017
51. Li HH, Hummon AB (2011) Imaging mass spectrometry of three-dimensional cell culture systems. Anal Chem 83(22):8794–8801. doi:10.1021/ac202356g
52. Watrous JD, Phelan VV, Hsu CC, Moree WJ, Duggan BM, Alexandrov T, Dorrestein PC (2013) Microbial metabolic exchange in 3D. Isme J 7(4):770–780. doi:10.1038/ismej.2012.155
53. Trede D, Schiffler S, Becker M, Wirtz S, Steinhorst K, Strehlow J, Aichler M, Kobarg JH, Oetjen J, Dyatlov A, Heldmann S, Walch A, Thiele H, Maass P, Alexandrov T (2012) Exploring three-dimensional matrix-assisted laser desorption/ionization imaging mass spectrometry data: three-dimensional spatial segmentation of mouse kidney. Anal Chem 84(14):6079–6087. doi:10.1021/ac300673y
54. Sinha TK, Khatib-Shahidi S, Yankeelov TE, Mapara K, Ehtesham M, Cornett DS, Dawant BM, Caprioli RM, Gore JC (2008) Integrating spatially resolved three-dimensional MALDI IMS with in vivo magnetic resonance imaging. Nat Methods 5(1):57–59. doi:10.1038/nmeth1147
55. Eberlin LS, Ifa DR, Wu C, Cooks RG (2010) Three-dimensional visualization of mouse brain by lipid analysis using ambient ionization mass spectrometry. Angew Chem-Int Ed 49(5):873–876. doi:10.1002/anie.200906283
56. Eberlin LS, Ferreira CR, Cooks RG (2012) Three-dimensional chemical imaging of a whole pig fetus by desorption electrospray ionization mass spectrometry. Reprod Fertil Dev 24(1):144–145
57. Nemes P, Barton AA, Vertes A (2009) Three-dimensional imaging of metabolites in tissues under ambient conditions by laser ablation electrospray ionization mass spectrometry. Anal Chem 81(16):6668–6675. doi:10.1021/ac900745e
58. Spraggins JM, Caprioli R (2011) High-speed maldi-tof imaging mass spectrometry: rapid ion image acquisition and considerations for next generation instrumentation. J Am Soc Mass Spectrom 22(6):1022–1031. doi:10.1007/s13361-011-0121-0
59. Roach PJ, Laskin J, Laskin A (2010) Nanospray desorption electrospray ionization: an ambient method for liquid-extraction surface sampling in mass spectrometry. Analyst 135(9):2233–2236. doi:10.1039/c0an00312c
60. Roach PJ, Laskin J, Laskin A (2010) Molecular characterization of organic aerosols using nanospray-desorption/electrospray ionization-mass spectrometry. Anal Chem 82(19):7979–7986. doi:10.1021/ac101449p
61. Nguyen TB, Roach PJ, Laskin J, Laskin A, Nizkorodov SA (2011) Effect of humidity on the composition of isoprene photooxidation secondary organic aerosol. Atmos Chem Phys 11(14):6931–6944. doi:10.5194/acp-11-6931-2011
62. Eckert PA, Roach PJ, Laskin A, Laskin J (2012) Chemical characterization of crude petroleum using nanospray desorption electrospray ionization coupled with high-resolution mass spectrometry. Anal Chem 84(3):1517–1525. doi:10.1021/ac202801g
63. Laskin J, Eckert PA, Roach PJ, Heath BS, Nizkorodov SA, Laskin A (2012) Chemical analysis of complex organic mixtures using reactive nanospray desorption electrospray ionization mass spectrometry. Anal Chem 84(16):7179–7187. doi:10.1021/ac301533z
64. Laskin J, Heath BS, Roach PJ, Cazares L, Semmes OJ (2012) Tissue imaging using nanospray desorption electrospray ionization mass spectrometry. Anal Chem 84(1):141–148. doi:10.1021/ac2021322
65. Lanekoff I, Heath BS, Liyu A, Thomas M, Carson JP, Laskin J (2012) Automated platform for high-resolution tissue imaging using nanospray desorption electrospray ionization mass spectrometry. Anal Chem 84(19):8351–8356. doi:10.1021/ac301909a
66. Lanekoff I, Thomas M, Carson JP, Smith JN, Timchalk C, Laskin J (2012) Imaging nicotine in rat brain tissue by use of nanospray desorption electrospray ionization mass spectrometry. Anal Chem 85(2):882–889. doi:10.1021/ac302308p
67. Lanekoff I, Burnum-Johnson K, Thomas M, Short J, Carson JP, Cha J, Dey SK, Yang PX, Conaway MCP, Laskin J (2013) High-speed tandem mass spectrometric in situ imaging by nanospray desorption electrospray ionization mass spectrometry. Anal Chem 85(20):9596–9603. doi:10.1021/ac401760s
68. Watrous J, Roach P, Heath B, Alexandrov T, Laskin J, Dorrestein PC (2013) Metabolic profiling directly from the petri dish using nanospray desorption electrospray ionization imaging mass spectrometry. Anal Chem 85(21):10385–10391. doi:10.1021/ac4023154
69. Laskin A, Laskin J, Nizkorodov SA (2012) Mass spectrometric approaches for chemical characterisation of atmospheric aerosols: critical review of the most recent advances. Environ Chem 9(3):163–189. doi:10.1071/en12052
70. Lanekoff I, Thomas M, Laskin J (2014) Shotgun approach for quantitative imaging of phospholipids using nanospray desorption electrospray ionization mass spectrometry. Anal Chem 86(3):1872–1880. doi:10.1021/ac403931r
71. Lanekoff I, Stevens SL, Stenzel-Poore MP, Laskin J (2014) Matrix effects in biological mass spectrometry imaging: identification and compensation. Analyst 139(14):3528–3532. doi:10.1039/c4an00504j
72. Lanekoff I, Thomas M, Carson JP, Smith JN, Timchalk C, Laskin J (2013) Imaging nicotine in rat brain tissue by use of nanospray desorption electrospray ionization mass spectrometry. Anal Chem 85(2):882–889. doi:10.1021/ac302308p
73. Thomas M. Heath BS. Laskin J. Dongsheng L. Liu E, Hui K. Kuprat AP. Kleese van Dam K. Carson JP Visualization of high resolution spatial mass spectrometric data during acquisition. In: Engineering in Medicine and Biology Society (EMBC), 2012 Annual International Conference of the IEEE, Aug. 28 2012-Sept. 1 2012. pp 5545–5548. doi:10.1109/EMBC.2012.6347250
74. Cha JY, Sun XF, Dey SK (2012) Mechanisms of implantation: strategies for successful pregnancy. Nat Med 18(12):1754–1767. doi:10.1038/nm.3012
75. Arima N, Uchida Y, Yu RX, Nakayama K, Nishina H (2013) Acetylcholine receptors regulate gene expression that is essential for primitive streak formation in murine embryoid bodies. Biochem Biophys Res Commun 435(3):447–453. doi:10.1016/j.bbrc.2013.05.006

76. Laasberg T, Neuman T (1985) Changes in the acetylcholinesterase and choline acetyltransferase activities in the early development of the chick embryo. Wilhelm Roux' Archiv 194(5):306–310. doi:10.1007/BF01152177
77. Gustafson T, Toneby M (1970) On the role of serotonin and acetylcholine in sea urchin morphogenesis. Exp Cell Res 62(1):102–117. doi:10.1016/0014-4827(79)90512-3
78. Drews U (1975) Cholinesterase in embryonic development. Prog Histochem Cytochem 7(3):1–52
79. Fisher MC, Zeisel SH, Mar M-H, Sadler TW (2002) Perturbations in choline metabolism cause neural tube defects in mouse embryos in vitro. FASEB J 16(6):619–621. doi:10.1096/fj.01-0564fje
80. Chirala SS, Chang H, Matzuk M, Abu-Elheiga L, Mao J, Mahon K, Finegold M, Wakil SJ (2003) Fatty acid synthesis is essential in embryonic development: fatty acid synthase null mutants and most of the heterozygotes die in utero. Proc Natl Acad Sci 100(11):6358–6363. doi:10.1073/pnas.0931394100
81. Burnum KE, Cornett DS, Puolitaival SM, Milne SB, Myers DS, Tranguch S, Brown HA, Dey SK, Caprioli RM (2009) Spatial and temporal alterations of phospholipids determined by mass spectrometry during mouse embryo implantation. J Lipid Res 50(11):2290–2298. doi:10.1194/jlr.M900100-JLR200
82. Tian Z, Zhao ZA, Liang XH, Zhang XH, Sha AG, Zhang ZR, Yu YS, Yang ZM (2011) Expression and function of fatty acid-binding protein 4 during mouse decidualization. Fertil Steril 95(8):2749–U2418. doi:10.1016/j.fertnstert.2011.05.052